

THE STERILE-ACTIVE NEUTRINO FLAVOR MODEL: THE IMPRINT OF DARK MATTER ON THE ELECTRON NEUTRINO SPECTRA

ILÍDIO LOPES

Centro de Astrofísica e Gravitação – CENTRA, Departamento de Física, Instituto Superior Técnico – IST,
Universidade de Lisboa – UL, Av. Rovisco Pais 1, 1049-001 Lisboa, Portugal

and

Institut d’Astrophysique de Paris, UMR 7095 CNRS,
Université Pierre et Marie Curie, 98 bis Boulevard Arago, Paris F-75014, France

Draft version December 19, 2018

ABSTRACT

Contact interactions between sterile neutrinos and dark matter particles in a hidden sector have been suggested as a good solution to simultaneously resolve the dark matter problem and anomalies in neutrino experiments. In this non-standard particle physics model, sterile and active neutrinos change their through vacuum oscillations and matter (or Mikheyev–Smirnov–Wolfenstein) oscillations, in which the latter mechanism of flavor oscillation depends strongly on the concentration of dark matter in the Sun’s core. We found that a large concentration of dark matter in the Sun’s interior changes substantially the shape of ^8B and hep electron neutrino spectra, but has an insignificant impact on the other neutrino spectra (i.e., pp, pep, ^7Be and ^{15}O , ^{13}N and ^{17}F). The strength of the interaction of the dark matter particles with neutrinos depends on an effective coupling constant, G_χ , which is an analog of the Fermi constant for the hidden sector. By using the latest ^8B solar neutrino flux, we found that G_χ must be smaller than $0.5 \times 10^9 G_F$ for this particle physics model to be in agreement with the data.

Subject headings: Neutrinos – Sun:evolution – Sun:interior – Stars: evolution – Stars:interiors

1. INTRODUCTION

Never has new particle been proposed to solve so many problems in theoretical physics as the sterile neutrino. This particle is in the race to become the best candidate to resolve simultaneously some of the most fundamental problems in particle physics and cosmology (Abazajian 2017). The sterile neutrino occurs naturally in well-motivated extensions of the standard model of particle physics. Its existence emerges naturally in one of the simplest mechanisms to explain the origin of the light masses of active neutrinos, the so-called *see-saw* mechanism (e.g., Gell-Mann et al. 2013). More significantly, this particle improves the agreement between theory and observations in the two complementary fields of research: experimental particle physics and observational cosmology. Its potential success in resolving such problems should not be underestimated. Two of these highlights are worth mentioning.

First, the sterile neutrino can explain the origin of the anomalies observed in several neutrino experiments (Gariazzo et al. 2016). Over the years there have been several discrepancies from various short-baseline neutrino experiments (Aguilar et al. 2001; Aguilar-Arevalo et al. 2010; Mention et al. 2011; Zimmerman & MiniBooNE Collaboration 2012) that point to the possibility that the active neutrino flavor oscillation model is incomplete. This weakness of the neutrino oscillation model has led many studies to incorporate additional single states into the same framework (e.g., Maltoni & Schwetz 2007; Barger et al. 2012). Even the simplest sterile neutrino model, the 3+1 flavor oscillation model made of 3 active neutrinos (ν_e, ν_τ, ν_μ) and a single sterile neutrino ν_s , i.e., ($\nu_e, \nu_\tau, \nu_\mu, \nu_s$), parametrized by only two additional parameters – a mass square splitting and a sterile-active mixing angle – seems to be a good solution (Palazzo 2011). This popular model is able to resolve the anomalies from the Liquid

Scintillator Neutrino Detector (Aguilar et al. 2001) and Mini-BooNE (Aguilar-Arevalo et al. 2010), and also be consistent with the data coming from solar and atmospheric neutrino experiments, by choosing a mass-squared splitting of the order of 1eV^2 and a mixing angle of the order of 10^{-1} (Mention et al. 2011). Similar parameters are also seemingly required to reconcile the flux deficit of reactor antineutrinos (Mention et al. 2011). This interpretation has recently been challenged by An et al. (2017): it seems that although its effect is less pronounced, the anomaly persists (Hayes et al. 2017).

Second, sterile neutrinos were proposed to resolve some of the well-known disagreements between numerical simulations and observations in the formation of the large-scale structure in the universe (Dasgupta & Kopp 2014). The standard collisionless cold dark matter (CCDM) model predicts the formation of too much structure formation at certain cosmological scales, in direct conflict with astronomical observations (Young 2017). These differences have been identified in three cases: (i) the *galaxy cusp core problem*, the disagreement between the cuspy density profiles predicted by numerical simulations of CCDM and the core profiles found in dwarf galaxies (e.g., Moore 1994); (ii) the *the too-big-to-fail problem*, the fact that most large sub-halos in CCDM simulations are too massive to host the satellites of the Milky Way (Boylan-Kolchin et al. 2011); (iii) the *missing satellites problem*, wherein the number of satellites found in simulations of the Milky Way-sized halos disagrees with observations by roughly a factor 10 (Kauffmann et al. 1993).

Although the first set of problems is well resolved by sterile neutrinos, which suggests that these neutrino experimental anomalies can be explained by postulating a sterile neutrino with the following parameters: mass difference $\sim \text{eV}$ and a mixing angle ~ 0.1 (or 6°), a detailed study has shown that these sets of parameters do not fix completely the problem found in the formation of structure (Hamann et al. 2011;

Hannestad et al. 2014). To alleviate this difficulty, a new mechanism has been postulated, the existence of a hidden sector comprising dark matter particles and sterile neutrinos in which the interactions between them are mediated by a massive gauge boson. The term *hidden sector* reinforces the fact that these interactions happen outside the standard model of particle physics. The existence of gauge forces within the dark matter sector has been considered for a long time. Actually, many of these models have been tested and constrained using several cosmological and astrophysical observational data sets (e.g., Jaeckel & Ringwald 2010). The possibility that these types of interactions can also occur with the neutrino sector seems a good one.

In this new class of cosmological models it is assumed that in the early universe there is an interaction between dark matter and sterile neutrinos, which, unlike typical cold dark matter candidates, keeps the dark matter kinetically coupled until a much later epoch. This change impacts the abundance of primordial elements during the Big Bang nucleosynthesis, modifies the cosmic microwave background (CMB), and alters the formation of large-scale structure, eliminating the conflict between simulations and data (Planck Collaboration et al. 2016). Moreover, the observational galactic problems mentioned above, such as the creation of dark matter cusps in the core of galaxies and a surplus of galaxies in the Local Group are successfully resolved in these cosmological models, which, unlike the standard cosmological model, do not lead to an excess in the formation of structure (Hooper et al. 2007; Cherry et al. 2014; Bertoni et al. 2015). This better agreement between observations and the theory is mainly due to the oscillations between active and sterile neutrinos.

As previously mentioned, sterile neutrinos are most likely created in the primitive universe (e.g., Babu and Rothstein 1992) or inside stars (e.g., Lopes 2018), either as the final product of the annihilation of dark matter particles or as a result of neutrino flavor oscillations. Indeed, these neutrinos appear to be the final state of annihilating dark matter in many explicit particle physics models previously considered in the literature (e.g., Garcia-Cely and Heeck 2017), and in other cases these are actually the dominant annihilation channel for dark matter (e.g., Dong et al. 2014). In any case, these neutrinos must have a mass below 10^3 TeV (Bambhaniya et al. 2017), a mass range that easily encompasses the expected mass of many dark matter particle candidates (Baer et al. 2015). The most important aspect of the class of particle physics models that is being considered in this study is the fact that neutrinos must interact at least in part with the dark matter, hence opening a window to this hidden sector.

The propagation of neutrinos throughout space may be affected by hypothetical couplings to the cosmic medium, such as dark matter, dark radiation, and dark energy. This challenging question has been addressed by many authors (Cirelli and Strumia 2006; Cui et al. 2018; Ghosh et al. 2018). Recently, Capozzi et al. (2018b) found that the next generation of detectors such as the Neutrino Telescope (KM3NeT, e.g., Adrián-Martínez et al. 2016) and IceCube Neutrino Observatory (IceCube, e.g., Aartsen et al. 2017) have the necessary sensitivity to probe many of the proposed non-standard interactions of neutrinos. Capozzi et al. (2018b) found these effects can be constrained to a level of a few per cent on the Earth's matter potential with coupling mediated by the μ -neutrinos. Moreover, baseline experiments such as Deep Underground Neutrino Experiment (e.g., LBNE Collaboration et al. 2013)

may provide additional complementary constraints on neutrino properties in the dark sector. Following the same strategy, these authors have shown that solar neutrino data can be used to put constraints on the 3+1 neutrino model in which neutrinos interact with dark matter by means of a Mikheyev–Smirnov–Wolfenstein (MSW) mechanism (Capozzi et al. 2017). They found that such modifications affect ^8B and carbon–nitrogen–oxygen (CNO) neutrinos.

The Sun and sun-like stars have been used quite robustly to impose constraints on large number of dark matter models (Turck-Chièze and Lopes 2012). This is possible because the accumulation of dark matter inside the star changes locally the transport of the energy affecting its whole structure, especially the core. Indeed, Lopes et al. (2002) have shown that the presence of dark matter significantly modifies the local luminosity of the star's core by changing the sound speed and temperature profiles, leading to the possibility of placing stringent constraints on such dark matter models using observational astronomical data. This is done in the Sun's case by comparing results of stellar models with helioseismic observations and data on solar neutrino flux, and in the case of sun-like stars by comparing with asteroseismic observations (Turck-Chièze and Lopes 2012). In recent years a multitude of different dark matter particle candidates have been suggested, all of which are able to affect the structure of the star. Nevertheless, depending on the specific properties of the dark matter particles, they can produce more or less significant changes. For instance, several authors have shown that self-interacting asymmetric dark matter can significantly enhance the accretion of dark matter by the star (Cumberbatch et al. 2010; Frandsen and Sarkar 2010; Taoso et al. 2010; Lopes and Silk 2012). Alternatively, Lopes et al. (2014) suggest that an asymmetric dark matter particle with a momentum-dependent scattering cross section could improve the agreement between the solar model and the helioseismic data, resolving the solar composition problem (Vincent et al. 2016). In addition, the Sun is no longer the only star we use to constrain the properties of dark matter. Casanellas and Lopes (2011) show that the oscillations of sun-like stars can be used as diagnostics to constrain the properties of dark matter further. In a follow-up to this work, the same group have reported the first asteroseismic constraints for asymmetric dark matter models (Casanellas and Lopes 2013; Martins et al. 2017). Equally, many other dark matter models have been presented in the literature (e.g., Kouvaris and Tinyakov 2011; Leung et al. 2012).

The standard theory of neutrino flavor oscillations based on three massive neutrinos (e.g., Gonzalez-Garcia and Maltoni 2008; Bilenyk 2010), is well established although it has a few, but important caveats that have motivated the appearance of alternative theories such as the one discussed in this article. Recent up-to-date reviews on the current status of the global analysis of data coming from neutrino oscillation and non-oscillation experiments can be found in Gonzalez-Garcia et al. (2016) and Capozzi et al. (2018a). Indeed, several articles have recently addressed the possibility of the neutrino flavor oscillations being described by a more general model than the standard model of oscillations in three neutrino flavors. Two classes of generalizations have become very popular in the particle physics community: the possibility of the three neutrinos having non-standard interactions with quarks, through a generalized MSW mechanism (e.g., Davidson et al. 2003; Papoulias and Kosmas 2015) and 3 + 1 (sterile) neutrino flavor oscillation models (e.g., de Holanda & Smirnov 2004; Cirelli

et al. 2005).

In relation to both neutrino models, several constraints have been placed on their fundamental properties using data coming from experimental detectors and astrophysical and cosmological observations. In particular, the solar electron neutrino spectra were computed for both types of neutrino flavor models, i.e., for a three-neutrino flavor oscillation model with a generalized MSW mechanism (Lopes 2017), and the 3+1 neutrino flavor oscillation model (Lopes 2018). Nevertheless, there is a very important difference between these two class of models: it is the fact that in the 3+1 neutrino flavor model, not only will the usual solar electron neutrino spectrum be affected (as well as the μ - and τ - neutrino spectra), but a new solar sterile neutrino spectrum will be produced in the Sun through neutrino flavor oscillations (Lopes 2018).

In this article we are interested in studying how a particle physics model with a hidden sector comprising dark matter and sterile neutrinos (in which the two sectors are linked) can be probed by the next generation of solar neutrino detectors. This work uses the 3+1 neutrino model developed by Capozzi et al. (2017). However, in this work, we compute the electron neutrino spectra of all the leading solar neutrino sources for an up-to-date solar model. Specifically, by using an up-to-date stellar evolution code that incorporates the subroutines that accreted dark matter from the halo (Lopes et al. 2011), we compute a model in which the Sun evolves within a halo of asymmetric dark matter, for which we then compute the electron neutrino spectra of all the leading solar neutrino sources. This neutrino flavor model corresponds to a generalisation of the 3+1 neutrino flavor model (Lopes 2018), where the neutrinos can now experience oscillations with the dark matter particles inside the Sun by a new MSW mechanism in the hidden sector. The specific goal of this work is to look for distortions in the shape of electron neutrino spectra due to the interaction of dark matter particles with sterile neutrinos.

In this section we have presented a brief review of the arguments in favor of sterile neutrinos being part of the solution to resolve the dark matter problem. In section 2, we present the basic model to explain the existence of dark matter in the Sun's core. In section 3 we present the current model to study the impact of dark matter in the 3+1 sterile neutrino oscillation model. In section 4 we present the predictions of solar sterile neutrino spectra influenced by the presence of dark matter. In the final section 5 we discuss the implication of these results for the next generation of solar neutrino experiments.

2. BARYONS AND DARK MATTER IN THE SUN

The fact that present-day dark matter and baryonic densities are of the same order of magnitude has motivated the idea for a possible link between the baryonic and dark matter sectors (e.g., Zurek 2014). This link can be created by an asymmetry generated in one or both sectors that is then communicated between them, giving rise not only to the baryonic asymmetry, but also to a dark matter asymmetry (e.g., Lopes and Silk 2012). In such models of asymmetry dark matter, only dark matter particles exist at present day, because dark matter antiparticles vanished by annihilation with the former in the primitive universe. In general, to correctly estimate the number of dark matter particles trapped inside the Sun or a star it is necessary to consider the self-interaction of dark matter, because a larger number of already accumulated particles may increase the self-capture rate significantly. Dark matter models in the class were studied in the solar case by Frandsen

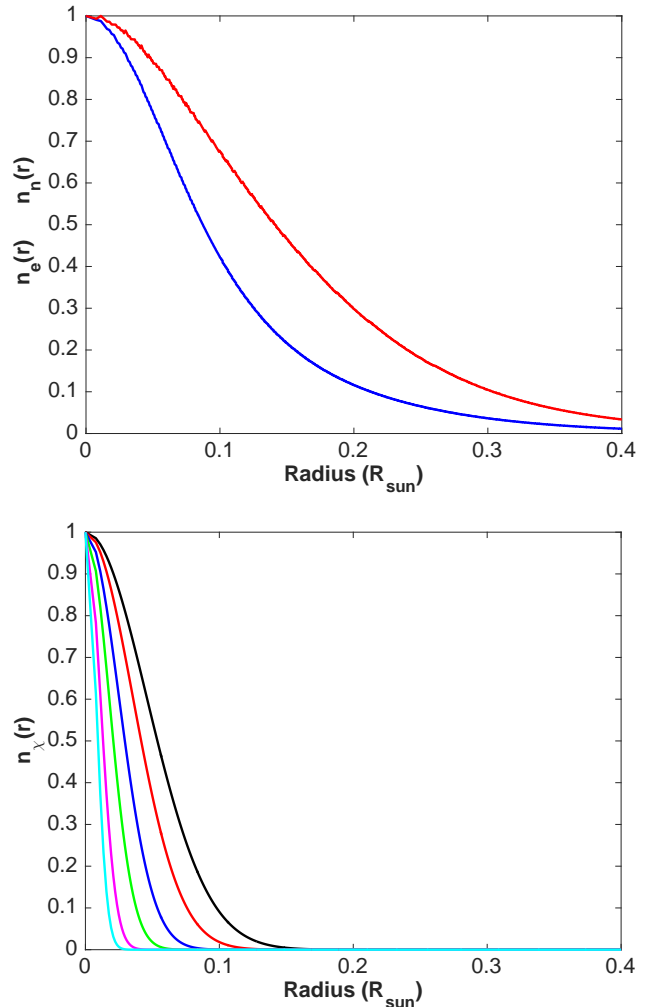


FIG. 1.— Variation of the number densities of electrons, neutrons, and dark matter particles for the present-day solar model. (a) The number densities of electrons $n_e(r)$ (red curve) and neutrons $n_n(r)$ (blue curve). The central values of n_e and n_n are $6.0 \times 10^{31} \text{ m}^{-3}$ and $2.7 \times 10^{31} \text{ m}^{-3}$. The values can change slightly with the properties of the dark matter halo. (b) The number density of dark matter particles $n_\chi(r)$ for $m_\chi = 3$ (black curve), 5, 10, 20, 50 and 100 GeV (cyan curve). To better illustrate the variation of the density functions with radius (in the Sun's core) we fix all central values to 1. For instance, for $n_\chi(r)$, at $r = 0$ we have $n_\chi(0) = n_{\chi c} = 1$.

and Sarkar (2010) and Taoso et al. (2010) and extended to other stars by Martins et al. (2017). However, in this study we will be conservative in our analysis, and as such we will only consider the capture of particles due to the interaction of dark matter with baryons.

2.1. Capture of dark matter by a star

As a star travels around the center of our Galaxy, it continuously captures particles from the halo of dark matter that encircles the Milky Way. The star's evolution is more or less affected, depending on the properties of such dark matter particles and the number of them accumulate in its interior. The impact of dark matter on the present structure of the star is regulated by the balance between the capture and annihilation of dark matter particles χ and antiparticles $\bar{\chi}$ inside it. The process of dark matter accumulation by the star can be summarized as follows: the dark matter particles of the halo may occasionally scatter with the nuclei of the different chemical elements present in the star's interior. If such collisions occur between the nuclei and dark matter particles, it may lead

to the dark matter particles losing enough energy to become trapped in the star’s gravitational field, an to end up by drifting to its center. Such a process that persists overtime ends up by modifying the evolutionary path of a star. Accordingly, the total number of particles and antiparticles, i.e, N_χ and $N_{\bar{\chi}}$, inside the star is determined by the balance between the capture rate and the annihilation rate of dark matter (e.g., [Jungman, Kamionkowski, & Griest 1996](#)). The values of N_χ and $N_{\bar{\chi}}$ at a given time of evolution are computed by solving the following system of coupled equations:

$$\frac{dN_i}{dt} = C_i - C_a N_\chi N_{\bar{\chi}}, \quad (1)$$

where i is equal to χ (dark matter particles) or $\bar{\chi}$ (dark matter antiparticles). In the above expression the evaporation of dark matter particles is neglected. The constant C_i gives the rate of capture of particles (antiparticles) from the dark matter halo and C_a gives the annihilation rate of particles and antiparticles. In general, the capture and annihilation of dark matter in the star’s core are relatively efficient processes; as such the final number of χ and $\bar{\chi}$ particles accreted by the star depends on the relative magnitude of the C_i and C_a processes. Since in this study we are considering only asymmetric dark matter, this corresponds to assuming that all antiparticles have annihilated with their counterparts in the primitive universe, and only χ particles have survived until the present day. It follows that the system of coupled equations (1) reduces to a single equation with $i = \chi$ and $C_a = 0$, i.e., $dN_\chi/dt = C_\chi$. Therefore over time N_χ increases in the core of the star, such that $N_\chi = C_\chi t$.

2.2. Evolution of the Sun in a halo of dark matter

The total number of dark matter particles present in the Sun’s core is calculated using a well established code to study the evolution of a star in a halo of dark matter. In this code the mechanism for the capture and energy transport of dark matter were implemented as explained in [Lopes et al. \(2011\)](#). This code was built by originally modifying the stellar evolution code CESAM ([Morel and Lebreton 2008](#)), a sophisticated code used to compute high-quality solar models. In particular, the code uses the equation of state and opacity coefficients from [Iglesias and Rogers \(1996\)](#), a Hopf solar atmosphere, and an adapted low-temperature opacity table. These models also included the appropriate screening, for which the Mitler prescription ([Dzitko et al. 1995](#)) is used, and also take into account the microscopic diffusion of helium and other chemical elements ([Brun et al. 1998](#)). See [Turck-Chièze et al. \(2004, 2010\)](#) and references therein for further details. The calculation of the solar models (with or without dark matter) is done using a set of input parameters that follow the well established criteria used to compute a standard solar model ([Turck-Chièze and Lopes 1993](#)). Each solar model evolves from the pre-main sequence until the present age of 4.5 Gyr. Typically in a scenario where a significant amount of dark matter is captured by the star, a single evolution model can have more than 140 time steps until it reaches the present age. Each solar model at a given epoch has more than 2000 layers. The stellar code requires that the structure equations are solved with an accuracy of 10^{-5} . In particular, the results of our modified solar model (e.g., [Lopes et al. 2011](#)) are in agreement with those of other codes in the literature (e.g., [Vincent et al. 2016](#)).

All solar models with or without dark matter are computed for an updated solar mixture of [Asplund et al. \(2009\)](#) by adjusting the initial helium content and the mixing length pa-

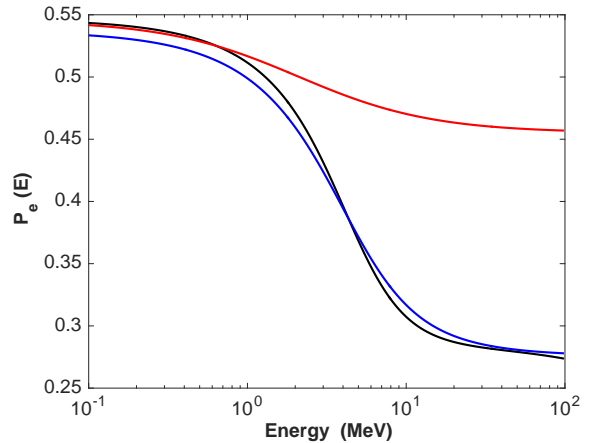


FIG. 2.— The survival probability of electron neutrinos: the P_e curves correspond to three neutrino models: three-flavor neutrino oscillation model (classical model; black curve); 3+1 flavor neutrino oscillation model (without dark matter; blue curve); 3+1 flavor neutrino oscillation model and dark matter with an effective strength of $G_\chi = 2.8 \times 10^{10} G_F$ (red curve).

rameter in such a way that at the present age of Sun ([Lopes and Silk 2013](#)) all the models reproduced the observed solar mass, radius, luminosity and Z/X surface abundance. Equally the solar model without dark matter is required to have an acoustic seismic spectrum and solar neutrino fluxes similar to other models found in the literature ([Turck-Chièze et al. 2010; Serenelli et al. 2011](#)). Moreover, the reference solar model used in our work is in full agreement with the standard picture of stellar evolution (e.g., [Turck-Chièze and Lopes 1993; Turck-Chièze et al. 2010; Serenelli et al. 2011](#)).

We have computed the evolution of the Sun in several dark matter particle scenarios, where m_χ takes the values 3, 5, 10, and 20 GeV. In agreement with recent constraints for spin-independent scattering cross section of the interaction of dark matter with baryons σ_{SI} , we choose the values 10^{-37} cm^2 for $m_\chi \sim 3 \text{ GeV}$ and 10^{-41} cm^2 for $10 \text{ GeV} \leq m_\chi \leq 100 \text{ GeV}$ ([Amole et al. 2017](#)). Similarly for the constraints on the spin-dependent scattering cross section of dark matter with baryons σ_{SD} , we choose the values 10^{-34} cm^2 for $m_\chi \sim 3 \text{ GeV}$ and 10^{-44} cm^2 for $10 \leq m_\chi \leq 100 \text{ GeV}$ ([Amole et al. 2017](#)). The other parameters used to define the properties of the dark matter halo can be found in [Lopes et al. \(2011\)](#); in particular, for the density of the dark matter we choose $\rho_\chi \sim 0.38 \text{ GeV cm}^{-3}$. These numerical simulations have produced several solar models for the present day, for which N_χ has taken values between 10^{37} and 10^{47} . The largest values correspond to a solar model with a large σ_{SI} value.

2.3. Electrons and neutrons

The propagation of neutrinos in matter is strongly dependent on the local distributions of electrons and neutrons. Figure 1 shows the density of electrons $n_e(r)$ and the density of neutrons $n_n(r)$ inside the Sun at the present age as predicted by an up-to-date standard solar model ([Lopes and Silk 2013](#)). The fact that $n_n(r)$ is much larger in the Sun’s center than at its surface results from the fact that more than 70% the Sun’s core at the present day consists ${}^4\text{He}$. Consequently, the Sun’s core has a larger number of neutrons than the more external layers, leading to a decrease in $n_n(r)$ from the center towards its surface. This important point is illustrated in Figure 1, which shows the relative density of electrons and neutrons inside the Sun. These quantities have a major impact on the propagation

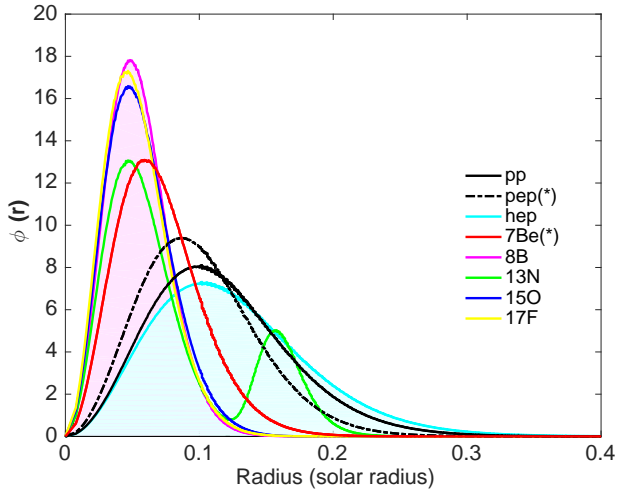


FIG. 3.— Neutrino emission sources of the various nuclear reactions of the proton-proton (pp) chain and carbon-nitrogen-oxygen (CNO) cycle present inside the Sun. The standard solar model used in this calculation is in good agreement with the helioseismology data, and its internal structure is identical to many other solar models found in the literature (see text). The figure shows the variation of the neutrino source $\phi_i(r)$ ($i = \text{pp}, \text{pep}(*), \text{hep}, {}^8\text{B}, {}^7\text{Be}(*), {}^{13}\text{N}, {}^{15}\text{O}$ and ${}^{17}\text{F}$) with the solar radius r . All the solar neutrino sources produce a continuous spectrum, with the exception of the $\text{pep}(*)$ and ${}^7\text{Be}(*)$ sources that generate spectral lines. The red and blue shaded areas correspond to the ${}^8\text{B}$ and hep sources, which are the most sensitive to the hidden sector (see text). Although solar models with dark matter will show a slight variation of the $\phi_i(r)$ functions, overall the $\phi_i(r)$ for solar models with and without dark matter will have similar. This figure was adapted from Lopes (2017).

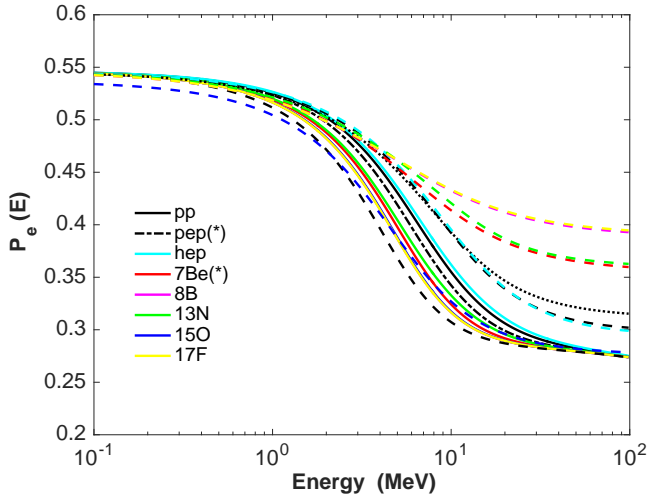


FIG. 4.— The variation of the different electron neutrino survival probability functions (P_e) with the energy of the emitted neutrino (the color scheme is the same one as in Figure 3): the continuous and dashed curves correspond to the standard model of three active neutrinos and to the 3+1 neutrino model with dark matter (see Figure 2). The P_e functions of the $\text{pep}(*)$ neutrino source are shown as black curve: a dotted-dashed line for the standard neutrino model and a dotted line for the 3+1 neutrino models.

of neutrinos, as we will discuss in the later sections. It is worth noticing that these quantities vary only slightly between solar models computed for different types of dark matter particles; the general form of these curves remains the same.

2.4. Dark matter particles

The accumulation of dark matter particles in the Sun's core during its evolution from the pre-main-sequence phase until its present age not only affects the structure of the core but, more importantly for this study, it also determines the number of

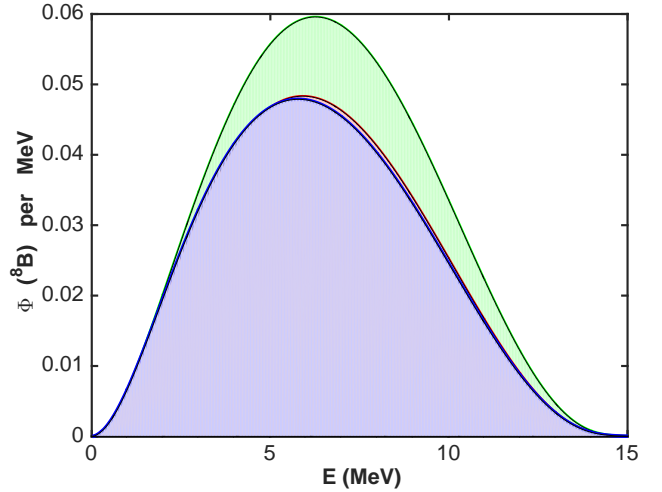


FIG. 5.— $\Phi_{8B, \odot}(E)$ is the electron neutrino spectrum for the present Sun in one of the following flavor neutrino oscillation models: (a) standard (three active neutrino) neutrino model (blue area); (b) 3+1 sterile neutrino model (red area); (c) 3+1 sterile neutrino model with dark matter with an effective strength of $G_\chi = 2.8 \times 10^{10} G_F$ (green area). In the calculation of these neutrino spectra we used an up-to-date standard solar model.

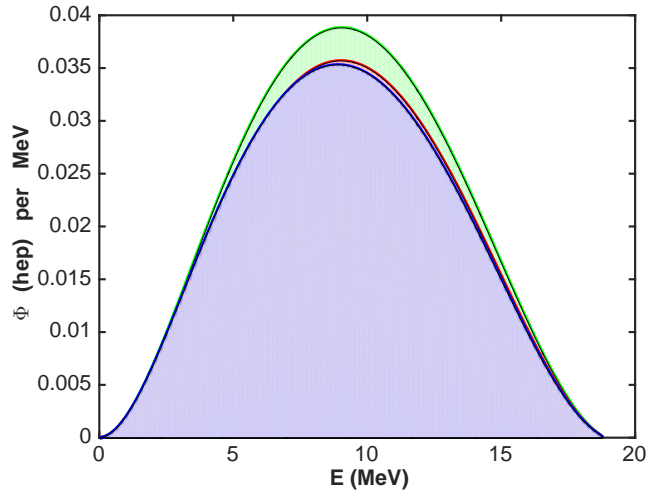


FIG. 6.— The electron neutrino spectrum of the hep neutrino source ($\Phi_{\text{hep}, \odot}(E)$) for the present Sun. The color scheme is the same as in Figure 5.

dark matter particles N_χ today. Nevertheless, the distribution of dark matter in the Sun's core is well approximated by the expression $n_\chi(r) = n_{\chi c} \exp(-\frac{r^2}{r_\chi^2})$ where $n_{\chi c}$ is the central density of dark matter particles and r_χ is the characteristic radius of the dark matter core. The quantity $n_{\chi c}$ depends on the total number of particles captured by the Sun at a fixed time N_χ (as given by Equation 1), for which $n_{\chi c} = N_\chi / (r_\chi^3 \pi^{3/2})$ with $r_\chi = \sqrt{3T_{c\odot} / (2\pi G_N \rho_{c\odot} m_\chi)}$ where $T_{c\odot}$ and $\rho_{c\odot}$ are the central temperature and density of the Sun. Two quantities affect $n_\chi(r)$ significantly: the values of N_χ and r_χ , both of which depend on the evolution of the Sun and can be obtained from the numerical simulations. Figure 1 shows the distribution of dark matter particles in the Sun's core for dark matter particles with different masses. It is quite clear that the more massive particles are concentrated in the Sun's core.

3. PROPAGATION OF STERILE NEUTRINOS INSIDE THE SUN

In the generalization of the standard model of neutrino flavour oscillations, i.e., that with three active neutrino fla-

vors, any number of sterile neutrinos are allowed to exist (e.g., [Palazzo 2011](#)). Nevertheless, even the simplest of these generalizations, in which the standard neutrino flavour model is extended to include only one sterile neutrino ν_s , i.e. the 3+1 sterile neutrino model ($\nu_e, \nu_\tau, \nu_\mu, \nu_s$), is sufficient to explain the neutrino anomalies mentioned previously ([Kopp et al. 2013](#)). In this case only two additional parameters are needed to define the flavor oscillation of ν_s : $|\Delta m_{41}^2|$ (the mass spilling) and θ_{14} (the mixing angle).

[Giunti et al. \(2013\)](#) have found that a global analysis of all the neutrino oscillation data sets can be fitted by a unique 3+1 neutrino model. These authors have found that in this case Δm_{41}^2 takes a value between 0.82 and 2.19 eV². This result was confirmed by an independent analysis of [Ko et al. \(2017\)](#) in which $|\Delta m_{41}^2|$ has similar values, i.e., $|\Delta m_{41}^2|$ varies between 0.2 and 2.3 eV². Similarly [Billard et al. \(2015\)](#) and [Ko et al. \(2017\)](#) found for the upper limit of θ_{14} the values: $10.6^\circ(0.1855)$ and $9.2^\circ(0.1582)$.

We could expect that the presence of dark matter in the Sun's core might affect the global analysis of neutrino oscillation data. Nevertheless, this effect is actually relatively small, since this global analysis depends marginally on the properties of the matter (by the MSW effect) in the core of the Sun. Therefore, even if the impact dark matter is such that it slightly affects the parametrization of the neutrino flavor model adopted, the main conclusions of this work will not change.

Accordingly, for this study we choose to adopt as fiducial parameters the values obtained by different authors by fitting the observational neutrino data to a 3+1 flavor neutrino oscillation model: $\Delta m_{21}^2 = (7.5 \pm 0.14) \times 10^{-5} \text{eV}^2$, $\sin^2(\theta_{12}) = 0.300 \pm 0.016$, and $\sin^2 \theta_{13} = 0.03$ from [Billard et al. \(2015\)](#); $\Delta m_{31}^2 = (2.457 \pm 0.047) \times 10^{-3} \text{eV}^2$ from [Gonzalez-Garcia et al. \(2016\)](#); and $\Delta m_{41}^2 = 1.6 \text{eV}^2$, $\theta_{14} = 0.1186$, $\theta_{24} = 0.1651$, $\theta_{34} = 0.000$, and all $\delta_{13,14,34} = 0$ from [Capozzi et al. \(2017\)](#). This last set of parameters is favored by short-baseline neutrino data. Moreover, we tested the sensitivity of the neutrino model to the parameters Δm_{21}^2 and θ_{12} by adopting the values found by [Capozzi et al. \(2017\)](#), and as expected the results found were identical to the previous ones.

3.1. The survival probability of electron neutrinos

The objective of this work is to compute the imprint of dark matter via sterile neutrinos on the spectrum of electron neutrinos produced by the Sun, specifically to identify how the shape of the neutrino spectrum changes due to the presence of dark matter in the Sun's interior. Fortunately, for the range of parameters we are interested in, the propagation of neutrinos from the Sun's core to the Earth takes a particularly simple form, since the evolution of neutrinos in space is identical to neutrino propagation in vacuum, and the propagation in matter is adiabatic. For that reason it is possible to compute the number of electron neutrinos arriving on Earth using a relatively simple formula (e.g., [Bilenky 2010](#)).

The evolution of the 3+1 neutrino flavor eigenstates ($\nu_e, \nu_\mu, \nu_\tau, \nu_s$) is governed by a Schrödinger-like equation. Following [Kuo and Pantaleone \(1989\)](#) conveniently, away from resonances, it is possible to compute the flavor oscillation by assuming a simplified picture of flavor oscillation of one sterile neutrino, ν_s , and an active one, which we chose to be ν_e . The motivation for such decomposition into two neutrino flavors is also discussed in [Lopes \(2018\)](#). This two-flavor neutrino model (ν_e, ν_s) is sufficient to explain the impact of the

dark matter in the 3+1 neutrino flavor oscillation model (e.g., [Palazzo 2011](#)). Among the several two-flavor neutrino models available in the literature that have been proposed to approximately compute the electron probability in the 3+1 neutrino model (e.g., [Lunardini and Smirnov 2000](#); [Miranda et al. 2015](#)), we choose the model obtained by [Capozzi et al. \(2017\)](#), which is in good agreement with the numerical solution. Thus, for a neutrino energy E , the evolution equation can be written as

$$i \frac{d}{dx} \begin{bmatrix} \nu_e \\ \nu_s \end{bmatrix} = \begin{bmatrix} V_x - \Delta c_{2\theta} & V_y + \Delta s_{2\theta} \\ V_y^* + \Delta s_{2\theta} & -V_x + \Delta c_{2\theta} \end{bmatrix} \begin{bmatrix} \nu_e \\ \nu_s \end{bmatrix}, \quad (2)$$

where $\Delta c_{2\theta} = (\Delta m_{21}^2/4E) \cos(2\theta_{12})$ and $\Delta s_{2\theta} = (\Delta m_{21}^2/4E) \sin(2\theta_{12})$, and V_x and V_y are functions related to the effective matter (ordinary and dark matter) potential inside the Sun. If we keep only the first-order terms, the survival probability P_e is

$$P_e = s_{13}^4 + c_{13}^4 c_{24}^4 s_{14}^4 + a_m + b_m, \quad (3)$$

where $c_{ij} = \cos \theta_{ij}$, $s_{ij} = \sin \theta_{ij}$, and a_m and b_m are dependent on the internal structure of the Sun. The functions a_m and b_m are given by the following expressions:

$$a_m = c_{13}^4 (c_{14}s_{12} - c_{12}s_{14}s_{24})^2 (c_{14}s_m - c_m s_{14}s_{24})^2$$

and

$$b_m = c_{13}^4 (c_{14}c_{12} + s_{12}s_{14}s_{24})^2 (c_{14}c_m + s_m s_{14}s_{24})^2,$$

with $c_m = \cos \theta_m$ and $s_m = \sin \theta_m$, where θ_m is the matter angle, which depends on the local distribution of baryons and dark matter particles inside the Sun. The function θ_m is given by

$$\cos(2\theta_m) = \frac{\mathcal{M}_x}{\sqrt{\mathcal{M}_y^2 + \mathcal{M}_x^2}}, \quad (4)$$

with $\mathcal{M}_x \equiv \cos(2\theta_{12}) - V_x$ and $\mathcal{M}_y \equiv |\sin(2\theta_{12}) + V_y|$ where V_x and V_y are functions related to the effective matter potential.

3.2. The effective matter potential

Neutrinos propagating throughout the Sun's interior will change flavor due to vacuum oscillations and matter oscillations. As the solar plasma is now composed of neutrons, protons, electrons, and dark matter particles, some of these particles will contribute to the neutrino flavor oscillation mechanisms. The interaction of neutrinos with the solar medium proceeds through coherent forward elastic charged-current (cc) and neutral-current (nc) scatterings; as usual, these effects are represented by the effective potentials V_{cc} and V_{nc} . These potentials are expressed as functions of local number densities $n_e(r)$ and $n_n(r)$:

$$V_{cc} = \sqrt{2} G_F n_e(r) \eta_\nu \quad (5)$$

and

$$V_{nc} = \sqrt{2} G_F \frac{1}{2} n_n(r) \eta_\nu, \quad (6)$$

where G_F is the Fermi constant and η_ν is the ratio of the neutrino energy E to Δm_{21}^2 given by $\eta_\nu(E) = 4E/\Delta m_{21}^2$. Δm_{21}^2 is computed as $\Delta m_{i1}^2 = m_i^2 - m_1^2$ ($i = 2, 3, 4$). Similarly, V_X is

the potential related to dark matter particles (Forastieri et al. 2017):

$$V_\chi(r) = G_\chi n_\chi(r) \eta_\nu, \quad (7)$$

where $G_\chi = \alpha_\chi g_B^2 / m_B^2$. This latter quantity is the equivalent of the Fermi constant in the hidden sector, for which g_B and m_B are the coupling constant and the mass of the hidden boson B , α_χ is a factor of the order of unity, which we will set to be one. In the calculation of V_χ we choose $G_\chi = 2.8 \times 10^{10} G_F$. This value comes from a constraint obtained from the CMB data (Forastieri et al. 2017).

The potential V_χ makes a significant impact on the 3+1 neutrino flavor model. This term introduces the mechanism by which dark matter can affect the variation of neutrino flavor. Its strength is regulated by the magnitude of G_χ .

The contributions of the effective matter potentials V_{cc} and V_{nc} and dark matter potential V_χ are taken into account in the previous Equation 4 thorough the expressions V_x and V_y :

$$V_x = \frac{1}{2} \left[V_{cc} c_{13}^2 \left(c_{14}^2 - s_{14}^2 s_{24}^2 \right) + V_s \left(s_{14}^2 - c_{14}^2 s_{24}^2 \right) \right] \quad (8)$$

and

$$V_y = \left(V_s - V_{cc} c_{13}^2 \right) c_{14} s_{14} s_{24}, \quad (9)$$

where $V_s = V_\chi - V_{nc}$.

The calculation of V_χ will be done for a specific model of dark matter. Since there is a large variation in the total number of dark matter particles with the properties of the dark matter, we choose the fiducial extreme value of $N_\chi \sim 10^{47}$ to illustrate the impact of dark matter on the 3+1 neutrino flavor model.

3.3. The survival of electron neutrinos

As in the classical neutrino flavor oscillation model, the conversion of electron neutrinos due to neutrino flavor oscillations depends on the local electron density $n_e(r)$ (Lopes & Turck-Chièze 2013), but this generalized neutrino flavor oscillation model also depends on the local neutron density $n_n(r)$ and the local dark matter density $n_\chi(r)$.

Figure 2 shows the variation of the $P_e(E)$ with the energy of the neutrino. P_e is given by Equation 3; the values of P_e are particularly accurate in the case that $s_{34} = 0$ and when $V_{cc} E / \Delta m_{31}^2 \ll 1$ (Capozzi et al. 2017). It is worth noticing that in relation to the standard model of three active neutrino model, the 3+1 model (without dark matter) affects equally the vacuum and matter of the electron neutrino, and the 3+1 model (with dark matter) affects most of the matter oscillations. In the latter model this effect is quite significant. The reason is related to the large value of G_χ adopted in these calculations. Indeed, while the standard model three active neutrinos and the 3+1 (without dark matter) neutrino model (Lopes 2018) have very similar survival electron probability P_e curves (compare black and blue curves), the 3+1 (with dark matter) neutrino flavor model has a P_e (red curve) clearly distinct from the previous models. This difference is more pronounced for neutrinos of higher energy (see Figure 2). An important aspect of this result worth highlighting is that the $P_e(E)$ sterile component (caused by the new parameters) affects electron neutrinos with any energy equally. However, the $P_e(E)$ dark matter component (related to the dark matter potential V_χ) affects mostly the neutrinos with higher energy. This last term is very sensitive to G_F and the N_χ .

4. THE SOLAR ELECTRON NEUTRINO SPECTRA

The solar electron neutrinos arriving on Earth are produced by the nuclear reactions of the proton-proton (PP) chains and the carbon-nitrogen-oxygen (CNO) cycle at very high temperatures in the deepest layers in the Sun's interior. Therefore to compute the neutrino spectra, we must take into account the location of neutrino sources inside the Sun. Thus to calculate the average survival probability of electron neutrinos for each nuclear reaction in the solar interior, i.e., $P_{e,i} \equiv \langle P_e(E) \rangle_i$, we compute

$$P_{e,i} = A_i^{-1} \int_0^{R_\odot} P_e(E, r) \phi_i(r) 4\pi \rho(r) r^2 dr, \quad (10)$$

where A_i is a normalization constant given by $A_i = \int_0^{R_\odot} \phi_i(r) 4\pi \rho(r) r^2 dr$, and $\phi_i(r)$ is the electron neutrino emission function for the nuclear reaction i . i corresponds to the following electron neutrino nuclear reactions: pp, pep, ^8B , ^7Be , ^{13}N , ^{15}O and ^{17}F (see figure 3). A detailed discussion about the neutrino sources inside the Sun, and the properties of these specific solar models can be found in Lopes (2013).

Figure 3 shows the local source of electron neutrinos for the standard solar model, which by definition is consistent with the current helioseismic and solar flux data. A detailed account of the properties of Equation 10 can be found in Lopes (2017). It is worth noticing that in general the dark matter affects significantly the evolution of the star in its core. Although the location of the different neutrino sources can vary with the dark matter, its effect on $\phi_i(r)$ is relatively small (see Figure 4). The electron neutrinos coming from the different nuclear reactions have a very similar behavior in terms of energy: neutrinos with relatively low energy are only affected by vacuum oscillations, while neutrinos with high energy are affected by vacuum and matter oscillations. Both of these effects are taken into account by the $P_e(E)$ function (Equation 3). Moreover, since neutrinos are produced in nuclear reactions located at different solar radii, the $P_{e,i}(E)$ curves vary slightly due to ϕ_i (Equation 10). This is the reason why in the standard neutrino flavor model the $P_{e,i}(E)$ are very similar for low- and high-energy neutrinos, with only small differences. However, if dark matter is present, while the difference is for the low-energy neutrinos, the effect is very large for very high-energy neutrinos. This is due to the contribution of $V_\chi(r)$ to $P_e(E)$ (see Figure 4). Actually, this is the reason why one could expect that neutrinos produced in nuclear reactions located near the center of the Sun, such as the neutrino sources ^8B and ^7Be (PP chains) and ^{13}N , ^{15}O and ^{17}F (CNO cycle), to be very affected by the presence of dark matter particles. Nevertheless, as we will discuss next, this is not necessary the case, because the neutrinos more affected are the ones produced near the Sun's center, but also the ones that have a relatively high energy.

Now that we have all the ingredients, then we can compute the electron neutrino energy spectrum of the different solar sources. The energy spectrum of electron neutrinos produced by a specific nuclear reaction in the Sun is essentially independent of the properties of the solar plasma at the location where occur nuclear reaction occurs. With a great degree of certainty we will consider that this neutrino spectrum is similar to the neutrino spectrum measured on laboratory on Earth for the same nuclear reaction. A typical example is the ^8B spectrum (e.g., Winter et al. 2006). Accordingly, we can use such an Earth spectrum as a reference against which we can test the new physics of our model. Hence, the difference

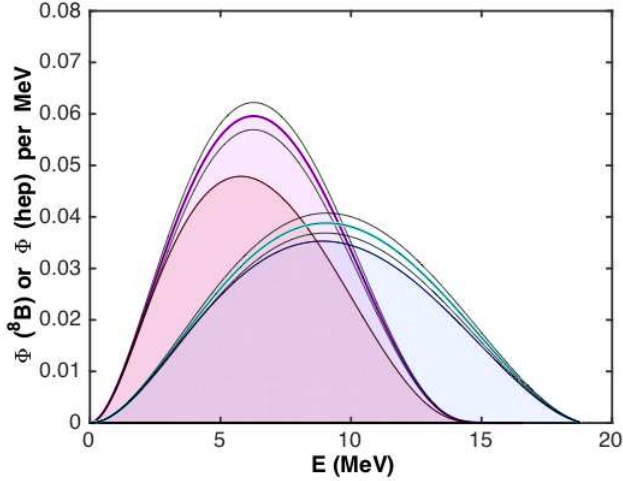


FIG. 7.— $\Phi_{8B,\odot}(E)$ (light red area) and $\Phi_{hep,\odot}(E)$ (light blue area) are the electron solar neutrino spectra for the 3+1 neutrino model with dark matter. The error bars are shown as thin black lines around the $\Phi_{8B,\odot}(E)$ and $\Phi_{hep,\odot}(E)$ curves. These black lines were computed assuming that $P_e(E)$ used to compute each of the $\Phi_{i,\odot}(E)$ spectra has an error of 0.1. This corresponds to the error associated with the electron survival probability of $P_e(E) = 0.29 \pm 0.1$ for an ${}^8\text{B}$ neutrino of energy 8.9 MeV (Bellini et al. 2010). For comparison, the $\Phi_{8B,\odot}(E)$ (dark red area) and $\Phi_{hep,\odot}(E)$ (dark blue area) curves that correspond to the three-neutrino model flavor model are also shown. Notice that the $\Phi_{8B,\odot}(E)$ and $\Phi_{hep,\odot}(E)$ for the three neutrino model flavor model are very similar to the ones corresponding to the 3+1 neutrino flavor model (without dark matter), as shown in Figures 5 and 6. For clarity we have not included the error bar in the standard neutrino model.

observed between the neutrino spectrum given by the nuclear reaction in the Sun’s core, $\Phi_i(E)$, and the neutrino spectrum that emerges from the Sun’s surface and is measured by a solar neutrino detector on Earth, $\Phi_{i,\odot}(E)$ is only due to neutrino flavor oscillations (either vacuum oscillations or vacuum-matter oscillations). Hence, the two previous neutrino energy spectra are simply related:

$$\Phi_{i,\odot}(E) = P_{e,i}(E)\Phi_i(E). \quad (11)$$

Figures 5 and 6 show two of these spectra. We notice that although several neutrino sources are located near the Sun’s center, only the spectra of ${}^8\text{B}$ electron neutrinos and hep electron neutrinos have their spectra modified by the presence of dark matter. This occurs because both sources produce neutrinos with relatively high energy. The effect is more pronounced in the ${}^8\text{B}$ electron neutrino spectrum because this neutrino source is located very near the core. The spectra of the other neutrino sources – pp, pep and ${}^7\text{Be}$ (pp chain reactions) and ${}^{13}\text{N}$, ${}^{15}\text{O}$ and ${}^{17}\text{F}$ (CNO cycle reactions) – are not shown because the effect of dark matter is negligible, i.e., these spectra are not affected by the presence of dark matter in the Sun’s core.

Figure 7 shows the error bars of the ${}^8\text{B}$ and hep spectra computed by assuming a realistic experimental error on the determination of these neutrino spectra. Accordingly, the error bars used in this calculation correspond to the maximum error estimated from the experimental errors on the neutrino fluxes computed by the different solar experiments, Borexino, SuperKamiokande, and SNO. Assuming the ${}^8\text{B}$ neutrino flux predicted by the high-metallicity standard solar model as used in this work, this corresponds to an electron survival probability of $P_e(E) = 0.29 \pm 0.1$ for a neutrino of energy 8.9 MeV (Bellini et al. 2010). The final error bars also include uncertainty coming from the mixing angles and mass

differences, as well as the theoretical uncertainty coming from the standard solar model. Moreover, the function $P_e(E)$ is only weakly sensitive to the physics of the solar model and is mostly affected through the variation of the radial distribution of electrons $n_e(r)$ or the radial density profile $\rho(r)$, which due to helioseismology is a quite robust quantity in the standard solar model. Therefore, the current uncertainties in the physics of the solar interior, such as the solar abundance metallicity problem, have a small impact in $P_e(E)$.

It follows from our analysis that in the case of the ${}^8\text{B}$ spectrum it is such that it is possible to distinguish between the 3+1 neutrino model (with dark matter) and the standard model of three active neutrinos. Therefore it is possible to distinguish between the two models. In the case of the hep neutrino spectra the distinction between the two models is not possible with the current set of data. Finally, we highlight the forthcoming next generation of neutrino experiments such as LENA (Wurm et al. 2012), for which a data set corresponding to five years of measurements will allow us to obtain an error four times smaller, i.e., $P_e(E) = 0.29 \pm 0.025$, for which these constraints will be much stronger.

5. DISCUSSION AND CONCLUSION

In this study, we have computed the expected alteration of the shape of the solar neutrino spectra expected to occur in a 3+1 flavor neutrino oscillation model due to the existence of dark matter in the Sun’s core. This new type of interaction, mostly due to the oscillations induced by dark matter as a result of a matter (MSW) oscillation mechanism in the hidden sector, depends on the specific properties of the dark matter particles, and also on the parameters of the neutrino flavor oscillation model. The most important factors affecting the neutrino flavors are the concentration of dark matter in the Sun’s core and the Fermi coupling constant of the hidden sector. There is also a small dependence on the local thermodynamic properties of the Sun’s core.

Nevertheless, it is worth mentioning that the solar neutrino spectrum for the 3+1 neutrino flavor oscillation model with dark matter presents significant differences from the standard three-neutrino flavor oscillation model, as well as from a non-standard neutrino flavor oscillation model such as the three-neutrino flavor oscillation model with a generalized MSW mechanism (Lopes 2017) and of the 3+1 neutrino flavor oscillation model (Lopes 2018). The neutrino flavor model discussed in this work is distinguished from the previous models mainly by the combination of two factors: the impact on the neutrino fluxes is limited to the Sun’s core, where the accumulation of dark matter occurs, and only neutrinos with a large energy are affected by neutrino flavor oscillations. It is the combination of these two effects that causes the 3+1 neutrino flavor model with dark matter to have a pronounced impact on the hep and ${}^8\text{B}$ neutrino spectra. This behavior is markedly different from the spectral variations found in the neutrino flavor oscillation model with a generalized MSW mechanism (Lopes 2017) and the 3+1 neutrino flavor oscillation model (Lopes 2018). In the first case, all the neutrino sources are affected. However, in the second case, an impact on the solar electron neutrino spectrum is predicted, as well a new solar sterile neutrino spectrum. Since dark matter particles inside the Sun are located very near the center, and only electron neutrinos emitted by the nuclear reactions with highest energy are affected, then the neutrino spectrum most modified is the spectrum emitted by the ${}^8\text{B}$ nuclear reaction.

The neutrino spectrum emitted by the hep nuclear reaction is similarly affected, although the effect is a smaller than in previous example. The impact of dark matter on the spectra of the other nuclear reactions is negligible.

Recently, Forastieri et al. (2017) used CMB observational data were able to constrain the Fermi coupling constant G_χ for the interactions of dark matter particles with sterile neutrinos (in the hidden sector). These authors found the following constraint: $G_\chi \lesssim 2.8 \times 10^{10} G_F$. In this study using the current ^8B neutrino flux measured by several solar neutrino detectors, and following a similar strategy to the previous work, we can put an independent constraint on the value of G_χ . Several neutrino experiments (e.g., Bellini et al. 2010; Agostini et al. 2017) have reported that the survival probability of electron neutrinos at $E = 8.9\text{MeV}$ is $P_e(E = 8.9\text{MeV}) = 0.29 \pm 0.1$. This value is consistent with the standard (three active) neutrino flavor oscillation model and the standard solar model.

We found that in order to obtain a P_e that is in agreement with the ^8B neutrino data, we must have $G_\chi \lesssim 0.5 \cdot 10^9 G_F$.

In conclusion, we have shown that if the neutrino spectroscopic measurements in the near future can be used to test new particle physics models, even possible interactions between sterile neutrinos and dark matter, the ^8B and hep electron neutrino spectra will be the best ones to use to look for this new type of phenomenon.

The author is grateful to the anonymous referee for the valuable comments and suggestions that improved significantly the contents and presentation of the article. The author thanks the Fundação para a Ciência e Tecnologia (FCT), Portugal, for the financial support to the Center for Astrophysics and Gravitation (CENTRA/IST/ULisboa) through the Grant No. UID/FIS/00099/2013.

REFERENCES

- Aartsen, M. G., and 307 colleagues 2017. *Physical Review D* 95, 112002.
- Abazajian, K. N. 2017, *Phys. Rep.*, 711, 1
- Adrián-Martínez, S., and 246 colleagues 2016. Letter of intent for KM3NeT 2.0. *Journal of Physics G Nuclear* 43, 084001.
- Aguilar, A., Auerbach, L. B., Burman, R. L., et al. 2001, *Phys. Rev. D*, 64, 112007.
- Agostini, M., Altenmuller, K., Appel, S., et al. 2017, [arXiv:1707.09279](https://arxiv.org/abs/1707.09279) [hep-ex].
- Aguilar-Arevalo, A. A., Anderson, C. E., Brice, S. J., et al. 2010, *Physical Review Letters*, 105, 181801.
- Amole, C., Ardid, M., Arnquist, I. J., et al. 2017, *Physical Review Letters*, 118, 251301.
- An, F. P., Balantekin, A. B., Band, H. R., et al. 2017, *Physical Review Letters*, 118, 251801.
- Astronomy and Astrophysics* 594, A13.
- Asplund, M., Grevesse, N., Sauval, A. J., Scott, P. 2009. *Annual Review of Astronomy and Astrophysics* 47, 481-522.
- Baer, H., Choi, K.-Y., Kim, J. E., Roszkowski, L. 2015. *Physics Reports* 555, 1-60.
- Babu, K. S., Rothstein, I. Z. 1992. *Physics Letters B* 275, 112-118.
- Bambhaniya, G., Bhupal Dev, P. S., Goswami, S., Khan, S., Rodejohann, W. 2017. *Physical Review D* 95, 095016.
- Barger, V., Gao, Y., & Marfatia, D. 2012, *Phys. Rev. D*, 85, 011302.
- Bellini, G., Benziger, J., Bonetti, S., et al. 2010, *Phys. Rev. D*, 82, 033006
- Bertoni, B., Ipek, S., McKeen, D., Nelson, A. E. 2015. *Journal of High Energy Physics* 4, 170.
- Bilenky, S. 2010. *Lecture Notes in Physics*, Berlin Springer Verlag 817.
- Billard, J., Strigari, L. E., & Figueroa-Feliciano, E. 2015, *Phys. Rev. D*, 91, 095023.
- Boylan-Kolchin, M., Bullock, J. S., Kaplinghat, M. 2011 *Monthly Notices of the Royal Astronomical Society* 415, L40-L44.
- Brun, A. S., Turck-Chièze, S., Morel, P. 1998. *The Astrophysical Journal* 506, 913-925.
- Capozzi, F., Lisi, E., Marrone, A., Palazzo, A. 2018. *Review Article on "Prog. Part. Nucl. Phys."*, [ArXiv e-prints arXiv:1804.09678](https://arxiv.org/abs/1804.09678).
- Capozzi, F., Shoemaker, I. M., Vecchi, L. 2018 *Journal of Cosmology and Astro-Particle Physics* 7, 004.
- Capozzi, F., Shoemaker, I. M., Vecchi, L. 2017. *Journal of Cosmology and Astro-Particle Physics* 7, 021.
- Casanellas, J., Lopes, I. 2011. *Monthly Notices of the Royal Astronomical Society* 410, 535-540.
- Casanellas, J., Lopes, I. 2013. *The Astrophysical Journal* 765, L21.
- Cirelli, M., Strumia, A. 2006. *Journal of Cosmology and Astro-Particle Physics* 12, 013.
- Cirelli, M., Marandella, G., Strumia, A., Vissani, F. 2005. *Nuclear Physics B* 708, 215-267.
- Cui, Y., Pospelov, M., Pradler, J. 2018. *Physical Review D* 97, 103004.
- Cumberbatch, D. T., Guzik, J. A., Silk, J., Watson, L. S., West, S. M. 2010. *Physical Review D* 82, 103503.
- Cherry, J. F., Friedland, A., Shoemaker, I. M. 2014. [ArXiv e-prints arXiv:1411.1071](https://arxiv.org/abs/1411.1071).
- Davidson, S., na-Garay, C. P., Rius, N., Santamaria, A. 2003. *Journal of High Energy Physics* 3, 011
- Dasgupta, B., & Kopp, J. 2014, *Physical Review Letters*, 112, 031803.
- de Holanda, P. C., & Smirnov, A. Y. 2004, *Physical Review D*, 69, 113002.
- Dong, P. V., Huang, D. T., Queiroz, F. S., Thuy, N. T. 2014. *Physical Review D* 90, 075021.
- Dzitko, H., Turck-Chièze, S., Delbourgo-Salvador, P., Lagrange, C. 1995. *The Astrophysical Journal* 447, 428.
- Forastieri, F., Lattanzi, M., Mangano, G., Mirizzi, A., Natoli, P., Saviano, N. 2017. *Journal of Cosmology and Astro-Particle Physics* 7, 038.
- Frandsen, M. T., Sarkar, S. 2010. *Physical Review Letters* 105, 011301.
- Garcia-Cely, C., Heck, J. 2017. *Journal of High Energy Physics* 5, 102.
- Gariazzo, S., Giunti, C., Laveder, M., Li, Y. F., Zavanin, E. M. 2016. *Journal of Physics G Nuclear Physics* 43, 033001.
- Gell-Mann, M., Ramond, P., Slansky, R. 2013. [ArXiv e-prints arXiv:1306.4669](https://arxiv.org/abs/1306.4669).
- Giunti, C., Laveder, M., Li, Y. F., & Long, H. W. 2013, *Physical Review D* 88, 073008.
- Gonzalez-Garcia, M. C., Maltoni, M., Schwetz, T. 2016. *Nuclear Physics B* 908, 199-217.
- Gonzalez-Garcia, M. C., Maltoni, M. 2008. Phenomenology with massive neutrinos. *Physics Reports* 460, 1-129.
- Ghosh, S., Khatri, R., Roy, T. S. 2018. *Physical Review D* 97, 063529.
- Iglesias, C. A., Rogers, F. J. 1996. *The Astrophysical Journal* 464, 943.
- Jaeckel, J., & Ringwald, A. 2010, *Annual Review of Nuclear and Particle Science*, 60, 405.
- Jungman, G., Kamionkowski, M., & Griest, K. 1996, *Phys. Rep.*, 267, 195.
- Ko, Y. J., Kim, B. R., Kim, J. Y., et al. 2017, *Physical Review Letters*, 118, 121802.
- Kouvaris, C., Tinyakov, P. 2011. *Physical Review Letters*, 107, 091301.
- Hamann, J., Hannestad, S., Raffelt, G. G., & Wong, Y. Y. Y. 2011, *Journal of Cosmology and Astroparticle Physics*, 9, 034.
- Hannestad, S., Hansen, R. S., Tram, T. 2014. *Physical Review Letters* 112, 031802.
- Hayes, A., Jungman, G., McCutchan, L., et al. 2017, [arXiv:1707.07728](https://arxiv.org/abs/1707.07728).
- Hooper, D., Kaplinghat, M., Strigari, L. E., Zurek, K. M. 2007. *Physical Review D* 76, 103515.
- LBNE Collaboration, and 485 colleagues 2013. [ArXiv e-prints arXiv:1307.7335](https://arxiv.org/abs/1307.7335).
- Lopes, I. 2013, *Physical Review D* 88, 045006.
- Lopes, I. 2017. *Physical Review D* 95, 015023.
- Lopes, I. 2018. *European Physical Journal C* 78, #327.
- Lopes, I. P., Silk, J., Hansen, S. H. 2002. *Monthly Notices of the Royal Astronomical Society* 331, 361-368.
- Lopes, I., Silk, J. 2012. *The Astrophysical Journal* 757, 130.
- Lopes, I., Silk, J. 2013. *Monthly Notices of the Royal Astronomical Society* 435, 2109-2115.
- Lopes, I., Kadota, K., & Silk, J. 2014, *The Astrophysical Journal Letters* 780, L15.
- Lopes, I., Panci, P., Silk, J. 2014. *The Astrophysical Journal* 795, 162.
- Lopes, I., Casanellas, J., Eugénio, D. 2011. *Physical Review D* 83, 063521.
- Leung, S.-C., Chu, M.-C., Lin, L.-M. 2012. *Physical Review D* 85, 103528.
- Lunardini, C., Smirnov, A. Y. 2000. *Nuclear Physics B* 583, 260-290.
- Kauffmann, G., White, S. D. M., Guiderdoni, B. 1993. *Monthly Notices of the Royal Astronomical Society* 264, 201.

- Kopp, J., Machado, P. A. N., Maltoni, M., Schwetz, T. 2013. *Journal of High Energy Physics* 5, 50.
- Kuo, T. K., Pantaleone, J. 1989. *Reviews of Modern Physics* 61, 937-980.
- Maltoni, M., & Schwetz, T. 2007, *Phys. Rev. D*, 76, 093005.
- Martins, A., Lopes, I., Casanellas, J. 2017. *Physical Review D* 95, 023507.
- Mention, G., Fechner, M., Lasserre, T., et al. 2011, *Phys. Rev. D*, 83, 073006.
- Miranda, O. G., Moura, C. A., Parada, A. 2015. *Physics Letters B* 744, 55-58.
- Moore, B. 1994. *Nature* 370, 629-631.
- Morel, P., Lebreton, Y. 2008. *Astrophysics and Space Science* 316, 61-73.
- Papoulias, D. K., Kosmas, T. S. 2015. *Advances in High Energy Physics* Volume 2015, Article ID 763648, s <http://dx.doi.org/10.1155/2015/763648>.
- Palazzo, A. 2011, *Phys. Rev. D*, 83, 113013.
- Serenelli, A. M., Haxton, W. C., Peña-Garay, C. 2011. *The Astrophysical Journal* 743, 24.
- Taoso, M., Iocco, F., Meynet, G., Bertone, G., & Eggenberger, P. 2010, *Physical Review D* 82, 083509.
- Turck-Chièze, S., Lopes, I. 1993. *The Astrophysical Journal* 408, 347-367.
- Turck-Chièze, S., Couvidat, S., Piau, L., Ferguson, J., Lambert, P., Ballot, J., García, R. A., Nghiem, P. 2004. *Physical Review Letters* 93, 211102.
- Turck-Chièze, S., Palacios, A., Marques, J. P., Nghiem, P. A. P. 2010. *The Astrophysical Journal* 715, 1539-1555.
- Lopes, I., & Turck-Chièze, S. 2013, *ApJ*, 765, 14 .
- Turck-Chièze, S., Lopes, I. 2012. *Research in Astronomy and Astrophysics* 12, 1107-1138.
- Young, B.-L. 2017. *Frontiers of Physics* 12, 121201.
- Vincent, A. C., Scott, P., Serenelli, A. 2016. *Journal of Cosmology and Astro-Particle Physics* 11, 007.
- Zimmerman, E. D., & MiniBooNE Collaboration 2012, *American Institute of Physics Conference Series*, 1441, 458.
- Zurek, K. M. 2014, *Physics Reports*, 537, 91.
- Winter, W. T., Freedman, S. J., Rehm, K. E., & Schiffer, J. P. 2006, *Phys. Rev. C*, 73, 025503
- Wurm, M., and 79 colleagues 2012. *Astroparticle Physics* 35, 685-732.